Korean J. Chem. Eng., 38(10), 2072-2081 (2021)
DOI: 10.1007/s11814-021-0847-8

pISSN: 0256-1115
eISSN: 1975-7220

Slow-rate devolatilization of municipal sewage sludge and texture of residual solids

Miloslav Hartman*,†, Bohumír Čech, Michael Pohořelý*,***, Karel Svoboda*, and Michal Šyc***

*Institute of Chemical Process Fundamentals of the Czech Academy of Sciences,
Rozvojová 135, 165 02 Praha 6, Czech Republic
**ENET Centre, Technical University of Ostrava, 17. listopadu 15, 708 33 Ostrava, Czech Republic
***Department of Power Engineering, University of Chemistry and Technology Prague,
Technická 5, 166 28 Praha 6, Czech Republic
(*Received 16 February 2021 • Revised 23 April 2021 • Accepted 16 May 2021*)

Abstract−Ash-rich sludge samples originating in four large plants were analyzed and employed to explore primarily the kinetics and the chemistry of devolatilization. A gravimetric, slowly increasing-temperature method was used in the range 298-1,123 K in a milieu of nitrogen. As an intricate combination of numerous (bio)organic and inorganic compounds, the dry sludge commences devolatilizing at approximately 418 K. The bulk of organic matter is released up to 823 K, at the rate becoming very slow thereafter. Basic constituents of the product gas are CO_2, CO, H_2, and CH_4 with undesired nitrogenous, sulfurous, and chloro compounds. The residual solids contain significant amounts of organic matter/carbon and, on account of their favorable textural characteristics, they can be viewed as promising sorbents or catalysts. Kinetic triad was inferred from the experimental data: the model is well-capable of simulating the process of devolatilization and can be used for design considerations. An explicit equation, based upon a tractable approximation to the temperature integral (for $[E/(RT)] \geq 0.1$), has been verified and proposed for predicting the maximum reaction rate temperature. Remarkable differences in thermal behavior were explored in detail between the sludge and the alkali bicarbonates.

Keywords: Sewage Sludge, Devolatilization, Thermogravimetry, Reaction Kinetics, Textural Features

INTRODUCTION

Municipal sewage sludge (MSS) is an arduous, semiliquid, and voluminous refuse originating from the mechanical-biological treatment of urban wastewater [1-3]. The sludge exiting the treatment process occurs in the form of a very dilute suspension, which contains on average about 5% of dry matter, composed largely of cell tissues and inorganic constituents. As is estimated, approximately 10 and 7.7 million metric tons (dry solids) are generated per annum in the EU and the US, respectively. These huge figures correspond to the rates of production as large as 53.5 and 64.5 g dry matter/(person day), respectively. Aside from domestic and rain (street) water, municipal plants also receive polluted water from a number of other sources such as hospitals, commercial, industrial, and agricultural enterprises. This wide variety of origins inevitably results in a variable and very complex chemistry of such a biogenic material as MSS.

Raw sludge is commonly stabilized, for example, through anaerobic (~55%) or aerobic digestion (~15%). Its anaerobic digestion is a sequential transformation process in which all unwanted organic material is converted into generally innocuous and well-dewatered solids with the aid of different acid- and methane-forming bacteria at slightly elevated temperature (~306 or 326 K). In this operation, about half the original matter is converted into a valuable digester gas composed mainly of methane (60-75% by vol.) and carbon dioxide. The stabilized sludge includes significant amounts of beneficial nutrient components. For example, the contents of organic nitrogen, phosphorus, and potassium are as high as about 25, 20, and 2 mg kg^{-1} dry matter, respectively. Unfortunately, the presence of heavy metals such as zinc (~500 mg kg^{-1} dry matter), copper, chromium (~50 mg kg^{-1} dry matter), lead, nickel, cadmium, mercury, and arsenic prevents the sludge from applying to agricultural or horticultural soils [3-5]. Combustion and co-combustion of sewage sludge [2,3,6-9] (e.g., with coal) make it possible to recover its energy potential that is similar to that of lignite: its higher heating value (HHV) amounts to approximately 10 MJ kg^{-1} dry matter. However, sludge incineration has not become up to the present a routine operation, particularly due to its high content of volatile matter (~40-50 wt%) and inorganic material/ash (~40-55 wt%), both on a moisture-free basis. Moreover, under practical conditions the fractional conversion of the reactive, organic-bound nitrogen to noxious NO_x (~$NO_{1.1}$) and N_2O amounts to about 0.1 and 0.05, respectively [3,10]. Furthermore, the concentration of nitrogen oxides in flue gas (~200-1,000 ppm (v)) occurs in inverse proportion to the concentration of carbon monoxide (50-200 ppm (v)). Of course, this creates a sort of dilemma over the choice of the incinerator temperature. Thus, in addition to the gaseous emissions of sulfur oxides and hydrogen chloride, those of nitrogen oxides must also be effectively removed to comply with the stringent, health regulations.

In an effort to avoid forming large quantities of flue gas and ash, novel thermal methods such as gasification (with a gasification medium) [7,11] and pyrolysis (also known as thermolysis, ther-

†To whom correspondence should be addressed.
E-mail: hartman@icpf.cas.cz

mal decomposition, devolatilization or partial gasification) [12-22] have been explored and developed. In essence, these mostly endothermic operations are based upon a series of physical and chemical transformations taking place when a complex (bio)organic material is exposed to an oxygen-starving milieu at ~473-1,223 K. During this process, the complex molecules break apart into simpler, more stable units by means of heating. In addition to light gases (e.g., CO_2, CO, H_2, hydrocarbons, and H_2O(g)), viscous oil and tar, and residual porous (bio)char rich in carbon are generally produced as well. Most products can be employed in a number of practical processes. As discovered in the past few years, an exposure of dry MSS to elevated temperature (~473-623 K) in some inert surroundings converts it into a hydrophobic and brittle product of considerably higher energy density and reactivity [10,23-26]. Such pretreatment, prior to further processing, is usually referred to as torrefaction, which also facilitates considerably the sewage sludge mechanical handling. For instance, torrefaction eases markedly problems of feeding the particulate sludge into pressurized gasifiers [10].

Very few kinetic studies on the MSS devolatilization have been reported in the literature [27-33] thus far. The behavior of sludge was mostly explored in terms of its origin and treatment under different heating conditions. Proposed models usually assume a number of parallel or overlapping decomposition reactions with the widely different activation energies and other reaction rate parameters. In the intense, contemporary search for a rational exploitation of the considerable, chemical and fuel potential of MSS, this study is aimed at (1) exploring the rate of the thermal decomposition of volatile organic matter contained in several municipal sewage sludges under well-defined conditions of experiment, and (2) unbiased modeling of this intricate phenomenon. An appropriate model is going to be a helpful tool for the rational design and operation of the novel thermal processes envisaged for sensible MSS utilization.

EXPERIMENTAL

The experimental work involved several segments: sludge sampling, treatment and preparation of samples, proximate, ultimate, and gas analyses, TGA experiments, and textural measurements.

1. Material and Particles

The sludge samples employed in this work were secured from four large, urban wastewater treatment plants. For instance, the largest of them produces about 90 metric tons of dry matter per day;

Table 1. Variation in proximate analyses of anaerobically digested sewage sludge produced by four municipal wastewater treatment plants[a]

Component, label	Range	Average
Volatile matter, VM	37.9-46.0	42.1
Fixed carbon, FC	5.0-12.3	8.2
Inorganic inert matter/ash, A′	47.5-54.0	49.7
Higher heating value, HHV, MJ kg^{-1}	10.4-11.9	11.2
Lower heating value, LHV, MJ kg^{-1}	9.6-11.0	10.4

[a]Given in wt% (on a moisture-free basis), the content of moisture amounts to 7.2 wt% (at 378 K)

Table 2. Variation in ultimate analyses of anaerobically digested sewage sludge produced by four municipal wastewater treatment plants[a]

Element	Range	Average
Carbon	23.8-26.6	25.4
Hydrogen	3.54-3.90	3.72
Nitrogen (organic)	2.24-2.97	2.58
Sulfur	0.47-0.86	0.73
Chlorine	0.05-0.22	0.16
Oxygen	15.4-20.6	17.6

[a]Given in wt% (on a moisture-free basis), the content of moisture amounts to 7.2 wt% (at 378 K)

the samples were withdrawn from the material which underwent thermophilic, anaerobic digestion at 323-329 K and was dewatered by means of high-speed centrifuges. All the samples were a dark brown color indicating the presence of metallic sulfides. The solids can be characterized as amorphous, nonplastic materials composed of granular as well as of colloidal components. All the samples emitted a characteristic tarry odor. The proximate and the elemental compositions of the sludge are documented in Tables 1 and 2, respectively.

Although there is some variation, the basic compositions of the tested samples are quite alike. Also, in all the samples the organic and the inorganic constituents are represented by practically equal parts. Results of the elemental analyses of the organic fraction provide an approximate empirical formula as follows:

$$C_6H_{10.5}N_{0.522}S_{0.065}Cl_{0.013}O_{3.11},$$

in which oxygen was estimated as a balance. This formula reminds of a glucose unit in the structure of the plant cell walls additionally laden with nitrogen, sulfur, and chlorine. As it was discovered, the amount of lignocellulose present in sewage sludge is generally low. Therefore, MSS is classified for the most part as a non-lignocellulose, biomass waste. The presence of significant amounts of nitrogen, sulfur, and chlorine implies forming a number of toxic and markedly malodorous compounds in exposure to elevated temperature (e.g., ammonia and amines, mercaptans, and chloro compounds).

In addition to the proximate and the ultimate analyses, the organic matter was also characterized by the gas chromatography (GC HP6890) and infrared spectroscopy (FTIR Equinox). Resulting chromatograms indicated the presence of large amounts of isometric, homologous, nonaromatic compounds, particularly hydrocarbons and their derivatives with the carbon numbers greater than ~10. The fraction of aromates was less than 10 wt%. IR spectroscopy identified the presence of organic acids, and their esters and salts. It also confirmed a large amount of inorganic material composed of silicates, phosphates, carbonates, and nitrates. The ash produced by firing the sludge in an oxidizing atmosphere at 1,173 K contained mainly SiO_2 (38.6 wt%), CaO (15.9 wt%), Al_2O_3 (13.1 wt%), Fe_2O_3 (12.7 wt%), P_2O_5 (10.7 wt%), MgO (3.3 wt%), and significant amounts of alkali metals. X-ray diffraction analyses revealed a variety of crystalline minerals such as quartz, hematite, feldspars, micas, apatites, and anhydrite.

On drying at 378 K to a constant mass, the sludge was slowly

ground with an agate mortar and pestle to obtain very fine specimens for the kinetic measurements. TGA experiments were conducted with a narrow fraction between 270 and 200 mesh by Tyler. The samples of the manually sieved particles were transferred into air-tight containers and stored in a refrigerator.

2. Apparatus and Procedures

As is well-known, unsteady-state methods of experiment approximate an isothermal, reaction regime quite closely; therefore, such a technique was employed. Moreover, the TGA method makes it possible to conveniently determine the reaction rate at any moment of time directly from the mass vs time data. To further minimize possible heat and mass transfer intrusions into the course of reaction, slow rates of heating (0.0167 deg s^{-1}), small mass (~7 mg) of finely sieved sludge particles (53-74 μm) were used in the experimental runs. To avoid thermodynamic constraints, a dry nitrogen flow of 0.833 cm^3 s^{-1} was maintained around the sample to ward off the gaseous products of reaction(s). Since the fumes released in the course of sludge devolatilization are particularly noxious and offensive, every effort was made to vent them effectively.

Devolatilization measurements were performed in a Setsys Evolution, Simultaneous TGA/DTA Analyzer (Setaram Corp.) provided with an Omni Star Spectrophotometer (Pfeiffer Vacuum Corp.). Temperature was increased at an invariant rate or was kept constant. The progress of devolatilization was evaluated in terms of the fractional conversion, X, as mass loss, $w_0 - w(\tau)$, at arbitrary temperature/time by means of Eq. (1):

$$X = \frac{1 - w'}{1 - w'_f} \tag{1}$$

The symbols w′ and w'_f represent the relative mass of sample at any moment of time and at the end of the process, respectively.

RESULTS AND DISCUSSION

1. Nonisothermal Kinetics

Besides water vapor, the product gas was composed mainly of CO_2 (monotonically disappearing with temperature), CO, and H_2 (both monotonically rising with temperature), and CH_4 (with a flat maximum at about 800 K) and tar (s).

Preliminary TGA experiments at a constant rate of temperature increase showed that the devolatilization takes place essentially in two steps: the principal part of organic matter is being released at temperatures up to ~823 K quite rapidly, but thereafter the process is going on very slowly. It can be of interest to note that the yield of desirable, condensed product(s) is relevant, while, for instance, toxic cadmium is not vaporized yet in the first stage. The tendency of dried sludge to decompose in a N_2 atmosphere was detected as very first mass loss at approximately 418 K. Both the small sample size and the slow rate of heating employed lend support to the relevance of this initial temperature of devolatilization. The starting product gas was composed largely of water vapor, carbon dioxide with a minor fraction of hydrogen and light hydrocarbons. Unfortunately, it was not possible to differentiate between the product and the educt water, the presence of which was quite likely. As is shown in Figs. 1 and 2, the devolatilization becomes relatively rapid at about 500 K, then slows and gradually comes to a virtual halt

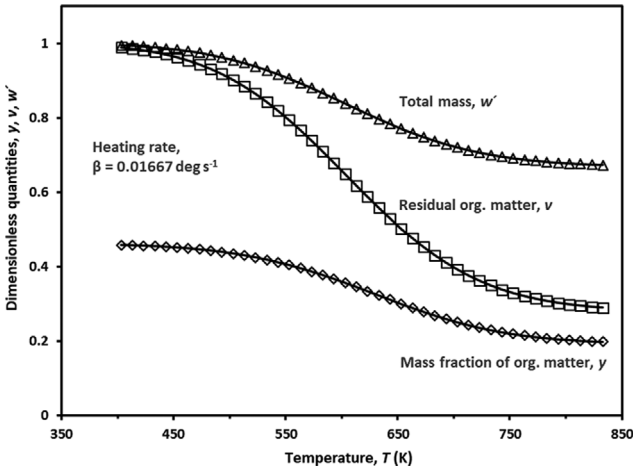

Fig. 1. Plots of normalized TG curves.

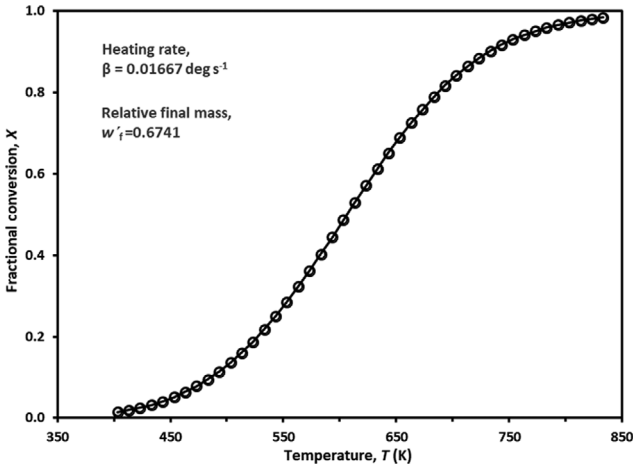

Fig. 2. Fractional extent of devolatilization vs thermodynamic temperature.

close to about 823 K at β=0.01667 deg s^{-1}.

In addition to the conversion, three other quantities were also employed to follow the course of devolatilization: the relative, total mass of solid residue, w′, the relative, residual amount of organic matter, v, and the mass fraction of organic matter in the solid residue, y. Mathematical definitions of these functions as well as their interrelationships, are presented in Nomenclature. Figs. 1 and 2 show the experimental and computed curves for these quantities in a range of 298-823 K. It should be mentioned that the experiments were replicated three times and the mean values are plotted in these above-mentioned figures. All of them are S-shaped, levelling off at ~823 K, and the final values of w′, v, and y are as large as 0.668, 0.277, and 0.192, respectively. As can be seen, a large majority of organic matter (72.3%) is released at such moderate temperatures with rather slow conversion thereafter. The amounts of the main components in the product gas released at 823 K (CO_2, CO, H_2, and CH_4) were in ratios of 1 : 0.23 : 0.62 : 0.26, respectively. Moreover, the selectivity to beneficial organic products (l), such as oils and tars, exhibited a maximum in the vicinity of this final temperature. Observations with the unaided eye did not reveal any

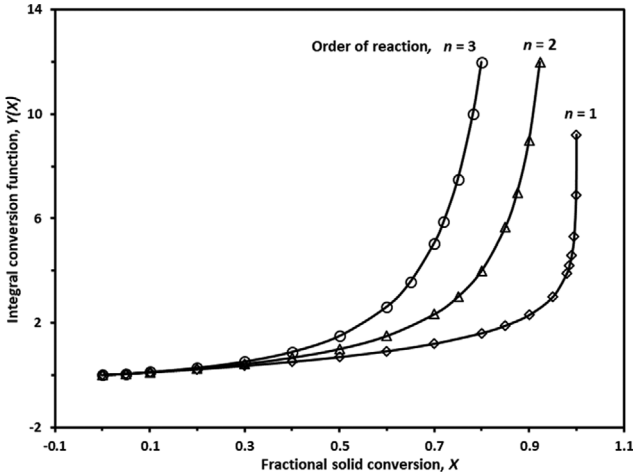

Fig. 3. Integral conversion function given by Eq. (2) as a function of the conversion and the order of reaction.

change in the size or in the shape of reacted solids; however, their original, dark grey surface turned black because of reaction(s).

Since the rate equation for the *n*th order reaction complies with most of the diffusion and the nucleation models, the integral conversion function, Y(X), can conveniently be written as

$$Y(X)\equiv\int_0^x \frac{dX}{(1-X)^n}=\frac{1-(1-X)^{1-n}}{1-n} \qquad \text{for } n\neq 1 \tag{2}$$

As is in detail documented in Fig. 3, the influence of the reaction order, n, on the function Y(X) is weak at early stages of reaction, i.e., for X<~0.2.

However, it gradually becomes highly relevant as the reaction progresses. The widely accepted Arrhenius' temperature dependency leads to the integral temperature function as follows:

$$Y(T)\equiv\frac{A}{\beta}\int_0^T e^{-\frac{E}{RT}}dT\cong\frac{AE}{\beta R}p(u) \tag{3}$$

where the right-hand side of Eq. (3) includes an approximation to the true integral. As is evident, the apparent/effective activation energy, E, occurs exclusively in the ratio E/R. Therefore, the would-be ambiguity of what mols are referred to in E does not have much relevance. With respect to equality of these two integral functions, the conversion, X, and the rate of reaction, dX/dT, can be expressed by

Table 3. Tested methods to approximate integral of Arrhenius temperature function $\int_0^T[\exp(-u)]dT\cong(E/R)p(u)$

Author(s)	Limitation	Approximation formula, p(u)
Coats and Redfern [29]	u≥35	$(1-2u^{-1})u^{-2}e^{-u}$
Schlömilch [30-32]	u≥25	$(2+u)^{-1}u^{-1}e^{-u}$
Cai et al. [33]	u≥5	$\frac{u+0.66691}{u+2.64943}u^{-2}e^{-u}$
Senum and Yang [34]	u≥1	$\frac{u^3+18u^2+86u+96}{u^4+20u^3+120u^2+240u+120}u^{-1}e^{-u}$
Vallet [35]	u≥1	Tables giving values of p(u) for $u\in\langle 1,200\rangle$
This work	u≥0.1	Equations in Table 4

Table 4. Approximation to Arrhenius temperature integral I(T)≅(E/R)p(u)=(E/R)exp(au+b)

Range of u	Polynomials for a and b				Range of p(u)
0.1-1	$a=-0.039019u^{-2}-1.123593u^{-1}-1.399777$ $b=0.032315(\ln u)^2-1.221626\ln u-0.620590$				7.22545E+00-1.48495E-01
1-5	$a=0.193099u^{-2}-1.631084u^{-1}-1.035817$ $b=-0.0993352(\ln u)^2-1.287596\ln u+0.571269$				1.48495E-01-1.99294E-04
5-10	$a=0.661123u^{-2}-1.868000u^{-1}-1.005154$ $b=-0.0949339(\ln u)^2-1.307261\ln u-0.591197$				1.99294E-04-3.83024E-07
10-20	$a=1.055614u^{-2}-1.948471u^{-1}-1.000991$ $b=-0.0734812(\ln u)^2-1.407342\ln u+0.708216$				3.83024E-07-4.702434E-12
	Coefficients k_i for $a=k_1u^{-1}+k_2$ and $b=k_3\ln u+k_4$				
	k_1	k_2	k_3	k_4	
20-30	−1.866357	−1.002538	−1.867651	1.429391	4.70243E-12-9.76556E-17
30-40	−1.900534	−1.001362	−1.901042	1.542211	9.76556E-17-2.53153E-21
40-50	−1.920617	−1.000852	−1.920866	1.615082	2.53153E-21-7.42357E-26
50-60	−1.930172	−1.000618	−1.932079	1.657004	7.42357E-26-2.35509E-30
60-70	−1.940229	−1.000449	−1.941816	1.696816	2.35509E-30-7.89076E-35
70-80	−1.947747	−1.000341	−1.949108	1.727769	7.89076E-35-2.75210E-39

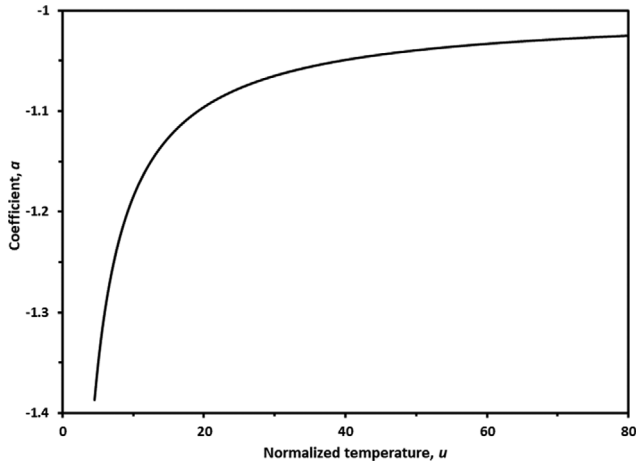

Fig. 4. Coefficient a in the integral approximation given by Eq. (6) and Table 4.

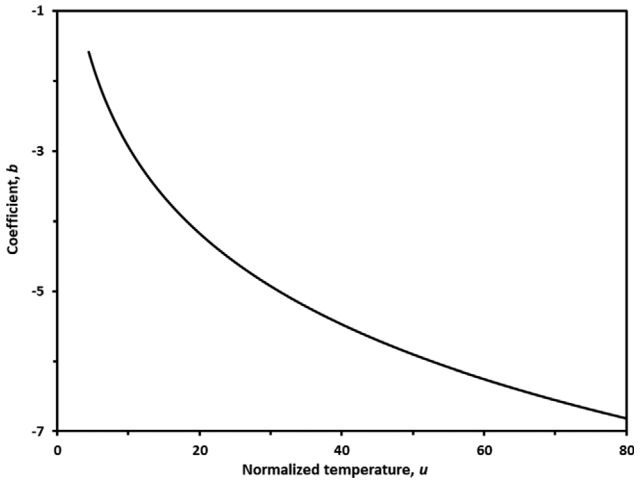

Fig. 5. Coefficient b in the integral approximation given by Eq. (6) and Table 4.

$$X=1-[1+(n-1)Y(T)]^{1/(1-n)} \quad (4)$$

and

$$\frac{dX}{dT}=[k(T)/\beta][1+(n-1)Y(T)]^{1/(1-n)} \quad (5)$$

A number of approximate equations were compared as potential substitutes for the analytically intractable integral of the Arrhenius exponential function. Some of these approximation formulae as well as the constraints upon them are given in Table 3.

One should realize that the devolatilization of organic materials takes place quite frequently under the conditions of u<~5. Unfortunately, the sole and lengthy integral approximation is available in such situations. Therefore, an alternate method was developed on the basis of Vallet's, eight-figure tables [35], which appear to be unrivalled as to their range (u∈⟨1,200⟩), as well as general accuracy. The final, multi-segment approximation to the Arrhenius integral in the convenient form

$$p(u)=\exp(au+b) \quad (6)$$

is summarized in Table 4.

The expressions for the coefficients a and b are visualized in Figs. 4 and 5, respectively.

As can be seen in these figures, both of the two coefficients are particularly sensitive to u<~20. Forty-four experimental data points at equal temperature intervals were employed to fit Eqs. (3) and (4). It turned out that the results obtained with the use of the Senum and Yang[34] approximation and with that given in Table 4 are practically equivalent. The values of the effective, kinetics triad (A, E/R, and n) were computed by the method of flexible polyhedron search (the simplex procedure) combined with the statistics using the Student "t" distribution. Results of the non-linear regression fitting are summarized in Table 5.

It is uneasy to compare these results to those in the literature. In addition to the different conditions of experiments, it is also due to the differences in data treatment. Thus, Urban and Antal [24] and Conesa et al. [25] present TGA curves that are more or less similar to those given in this work. However, the kinetic parameters reported by the aforesaid authors are appreciably different. For instance, a fairly involved model assumes up to six parallel/overlapping reactions, whose apparent activation energy terms, E/R, and orders, n, vary from 5,138 to 39,950 K and from 2 to 23, respectively. Therefore, it is hard to find a plausible explanation for such widely varying values.

The curve in Fig. 6 depicts the reaction rate in the course of increasing temperature and time. As is shown, the highest rate is attained at approximately 604 K and amounts to 4.12×10^{-3} K^{-1} (6.87×10^{-5} s^{-1}).

Biagini et al. [27] worked with a similar, dried sludge containing 45.6 wt% of inorganic matter. They determined a peak rate of devola-

Table 5. Effective kinetic parameters for thermal decomposition of dry, anaerobically digested sewage sludge in nitrogen environment[a]

Parameter	Value	95% confidence interval	Variance
Frequency factor, A, s^{-1}	9.39618×10^{-2}	$\pm1.362\times10^{-4}$	6.120×10^{-5}
Activation energy term, E/R, K	3.83044×10^{3}	±1.532	0.7212
Order of reaction, n	1.261	±0.0390	0.0156

[a]Deduced from the experiments conducted with the finely ground, 7 mg dry samples in a nitrogen flow of 0.85 cm^3 s^{-1} at a heating rate of 1.6667×10^{-2} deg s^{-1}, temperature range from 373 to 823 K. The data used come from three experimental runs replicated under the same process conditions. The approximation by Senum and Yang [34] to the Arrhenius integral was employed as well as that developed by the authors and given in Table 4

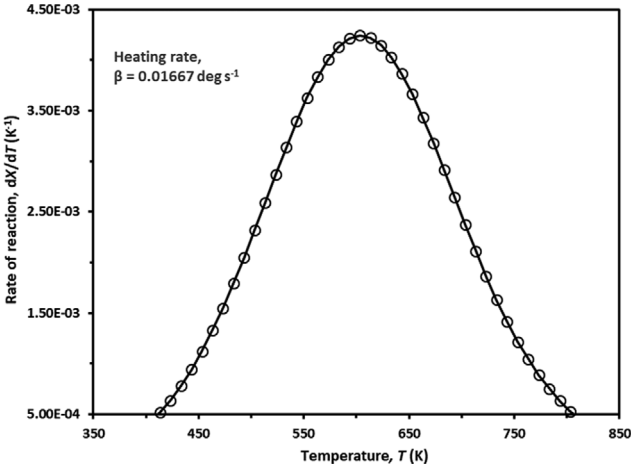

Fig. 6. Rate of devolatilization in the course of an increasing-temperature experiment.

tilization as large as 6.62×10^{-3} K^{-1} at 623 K. With respect to a considerably larger heating rate of the authors (β=0.333 deg s^{-1}) and to general sensitivity of the values of reaction rates, such an agreement appears to be fairly good.

The convenient form of Eq. (6) makes it possible to develop an explicit equation for predicting the point of maximum (peak) reaction rate on the curves in Figs. 2 and 6:

$$u_p=-a^{-1}\left\{\ln\left[\frac{AE}{\beta R}(1-n(a+1))\right]+b\right\} \quad (7)$$

As is evident, this equation can readily be employed in combination with the integral correlation embodied in Table 4.

2. Comparison with Potassium and Sodium Hydrogen Carbonate and Dissociation Pressures of Magnesium and Calcium Carbonate

Predictions of the above-presented expression compare quite well with the corresponding, experimental findings on MSS, $KHCO_3$ [36], and $NaHCO_3$ [37] in Table 6. But in stark contrast to MSS, the bicarbonates used were pure, crystalline, chemical individuals. Othman et al. [38] experimented with rather low-ash sludge and employed a DTG technique at higher rates of heating. The peak temperature, T_p, deduced from the authors' graphs amounts to approximately 623 K for β=0.0833 deg s^{-1}. On accounting for an inherent effect of β on the experimental rate curves, one gets a value T_p=~598 K, which is in fair agreement with the results given in Table 6 (T_p=604 K).

Experience indicates that it is meaningful to supplement the bare kinetic triad (A, E, and n) with other physical characteristics. Some additional, instructive quantities, such as the width of the (dX/dT) curve, the characteristic values of the integral functions, as well as the above-mentioned point of maximum reaction rate, were employed in comparison with $KHCO_3$ in Table 7.

The most striking difference occurs between the temperatures of the maximum reaction rates, i.e., T_p (MSS)–T_p ($KHCO_3$), and is as large as 182.2 deg. This difference corresponds to a value of −34.0 in terms of the normalized (reciprocal) temperature, u_p. It is worth mentioning that although the temperature of the maximum rate of MSS is larger than, e.g., that of $KHCO_3$ by a factor of 1.43, its reaction rate, $(dX/dT)_p$ is about eight times less than that of $KHCO_3$. There is at least one more point that deserves attention: the width of the derivative curve (dX/dT) vs T. While the difference between the temperatures at which $dX/dT=0.5(dX/dT)_p$ for MSS amounts to 217.4 deg, the corresponding value for $KHCO_3$ amounts to no more than 26.7 deg. Although these two quantities are remarkably different, they become quite close when expressed as the normalized temperatures, u_p: 2.33 (MSS) and 2.54 ($KHCO_3$). The integral temperature functions at the peak reaction rate, $Y(T_p)$, are significantly different and amount to 0.737 (MSS) and 0.946 ($KHCO_3$). On the other hand, there is a negligible difference in breadth of the considered rate curves in terms of the conversion, X, which amounts to ~0.74.

Table 6. Predictions of point of maximum reaction rate on kinetic curves by means of Eq. (7) and Table 4 for different substances

Reactant	Term AE/(βR)	Coefficients in Eq. (7)		Normalized temperature, u_p	Temperature, T_p, K	
		a	b		Eq. (7)	Experiment
MSS, this work	2.1595×10^4	−1.28329	−2.14731	6.3418	604	603.8
$KHCO_3$ [36]	5.0990×10^{20}	−1.04852	−5.48476	40.2950	421.9	423
$NaHCO_3$ [37]	8.4485×10^{15}	−1.06531	−4.90597	29.8802	406.9	409

Table 7. Comparison of decomposition rates of anaerobically digested sludge and potassium hydrogen carbonate in nitrogen atmosphere[a]

Quantity	Sludge	$KHCO_3$
Integral temperature function at maximum rate of reaction, $Y(T_p)$	0.73706	0.94572
Maximum rate of reaction, $(dX/dT)_p$, K^{-1}	4.2447×10^{-3}	0.034370
Conversion at maximum rate of reaction, X_p	0.49040	0.5878
Difference between temperatures at which $dX/dT=0.5(dX/dT)_p$, deg	217.4	26.7
Difference between normalized temperatures, u, at which $dX/dT=0.5(dX/dT)_p$	2.330	2.536
Difference between conversions at which $dX/dT=0.5(dX/dT)_p$	0.73951	0.73680

[a]Kinetic parameters for the sludge are presented in Table 5. Kinetic triplet for potassium hydrogen carbonate is as follows: $A=4.9992\times10^{14}$ s^{-1}, E=141.34 kJ mol^{-1}, and n=1.145 determined at $\beta=1.6667\times10^{-2}$ deg s^{-1} (ref. [36]). Temperatures u_p and T_p are given in Table 6.

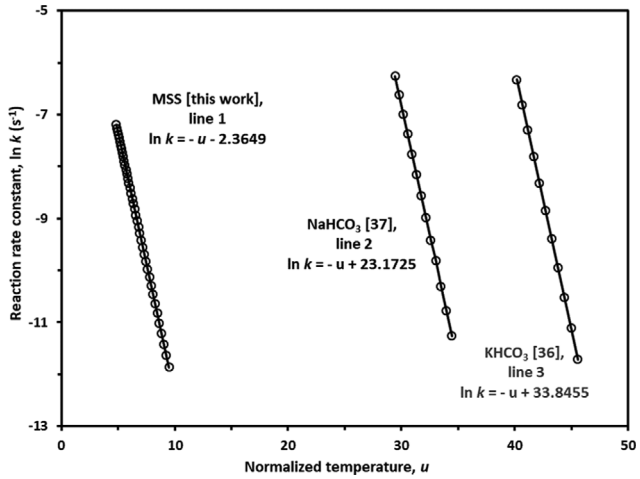

Fig. 7. Comparison of reaction rate constants for sewage sludge, sodium hydrogen carbonate, and potassium hydrogen carbonate.

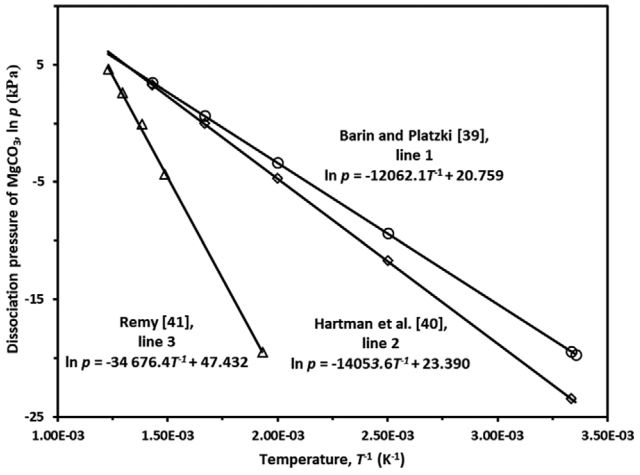

Fig. 8. Comparison of the dissociation pressure of magnesium carbonate as predicted by regression equations based upon different data.

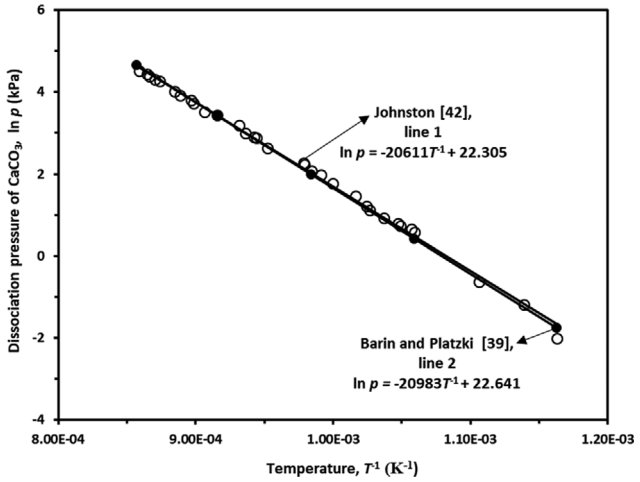

Fig. 9. Comparison of the dissociation pressure of calcium carbonate as predicted by regression equations based upon different data.

The experimental data, interpreted as the reaction rate constants, are compared in Fig. 7 with the results on the thermal decomposition of $KHCO_3$ [36] and $NaHCO_3$ [37].

As can be seen, the presented parallel lines are wide apart because of the greatly distinct pre-exponential factors, A ($\sim 10^{-2}$-10^{14} s^{-1}) as well as due to considerably different, normalized temperatures, u (~4-46). The acquired findings make it possible to explore the sensitivity of the reaction rate constants to temperature. If it is desired to augment the reaction rate constant, k, for instance, from 1.23×10^{-4} s^{-1} (ln k=−9) to 3.35×10^{-4} s^{-1} (ln k=−8), i.e., by a factor of 2.72, this is accomplished by adequate increases of temperature. Thus, it is necessary to raise the temperature of reaction for MSS, $NaHCO_3$, and $KHCO_3$ by 102.4, 12.1, and 9.5 deg, respectively, from T/u=577.3 K/6.64, 378 K/32.2, and 396.8 K/42.8. As is evident time and time again, the thermal behavior of MSS widely differs from that of $NaHCO_3$ and $KHCO_3$. Its considerably less activation energy as well as the much smaller pre-exponential factor must be borne in mind in this respect. These facts are also documented in Table 6 by the term AE/(βR), whose values for MSS, $NaHCO_3$ and, $KHCO_3$ range from 2.16×10^4 through 8.45×10^{15} to 5.1×10^{20}, respectively. Understandably enough, the primary reason for such differences lies with the greatly different and intricate chemistry of the sludge devolatilization.

It was found in separate bench scale experiments that the concentration of carbon dioxide in the product gas can reach tens of percent. Having in mind the relevant amounts of magnesium and calcium components present in solids, the question arises of fixing and/or releasing carbon dioxide, especially under the TGA conditions. The equilibrium dissociation pressures of CO_2 above magnesium carbonate and calcium carbonate are shown in Figs. 8 and 9, respectively.

While $MgCO_3$ tends to incipiently decompose ($\sim p_{CO_2}$=1 kPa) at 600.8 K (line 2 in Fig. 8), $CaCO_3$ commences dissociating at 926.8 K (line 2 in Fig. 9). The dissociation temperatures, at which p_{CO_2} is as large as an ambient pressure of 101.325 kPa, amount to 748.7 K (line 2 in Fig. 8) and 1,164.3 K (line 2 in Fig. 9), respectively. Thus, it can be inferred that no $MgCO_3$, but all $CaCO_3$ are most likely to remain in the solid residue exposed to a temperature of 823 K. As is known, the decomposition of small, fine-grained samples of the two carbonates is very rapid (if not instantaneous) at their aforesaid dissociation temperatures.

3. Textural Properties of Solid Residues

Microscopic examination of the solid carbonaceous residues devolatilized at 823 K did not reveal any significant thermoplastic behavior such as shrinkage of the reacted particles. Therefore, every mass loss brings about an adequate increase in porosity of the reacted particles. Having used the helium intrusion analysis and the mercury pycnometry, the true and the apparent densities of solids were determined as large as 2.20 and 0.836 g cm^{-3}, respectively. The corresponding pore volume, V_p, and the fractional porosity, e, amount to 0.742 cm^3 g^{-1} and 0.620, respectively. Moreover, the specific surface area of the reacted sludge, exposed to a temperature of 823 K for 1 h, was evaluated by BET analysis with the N_2-adsorption as large as 45.9 m^2 g^{-1}. Compared, for example, with the potas-

sium carbonate formed by the thermal decomposition of $KHCO_3$[36], the aforementioned value is about ten times greater than that for K_2CO_3. It is certainly of interest to notice that approximately half the surface area is constituted by the mesopores (2-50 nm in diameter). The surface area of the dry, unreacted sludge and that of its well-ignited ash amount to merely 6.0 and 2.1 $m^2\ g^{-1}$, respectively. As was found out, the residual solid is moderately alkaline and includes 19.1% by mass of carbon. Accordingly, the determined surface area can be for the most part ascribed to the residual carbon. One more point deserves serious consideration: initial results indicate that except for volatile mercury, the heavy metals are effectively encapsulated within the residual solids. Consequently, they are more resistant to the spontaneous lixiviation than those present, for instance, in the original sludge or in its ash. As follows from the above, the physicochemical properties of the devolatilized sludge residues (biochars) predetermine their use as inexpensive, carbonaceous sorbents in removal, for example, of mercaptans and acidic or phenolic pollutants from putrid gases and nuisance liquids. Furthermore, biochar can also be employed as an amendment to different types of soil to upgrade their properties.

4. Postlude

Fig. 10 provides a continuance of Fig. 1 and depicts the dimensionless characteristics w′, v, and y as functions of the operating temperature in the range 823-1,123 K.

In addition, the true/overall degree of devolatilization conversion, X_t, based upon the initial organic matter, 1−A′, is presented in this figure as well. It can be seen that all the explored quantities change gradually and at a very slow pace with temperature, more or less, in a linear manner. From a practical standpoint the residual biochar, exposed to a temperature of 1,123 K, still contains about 5.5 wt% of organic matter, i.e., X_t=0.929. As can easily be estimated, the mean rate of devolatilization is very low and amounts to approximately $6.94\times10^{-4}\ K^{-1}$, i.e., $1.16\times10^{-5}\ s^{-1}$. Having taken advantage of the results given in Figs. 1 and 10, it is clearly perceptible that the amount of organic matter released in the first and principal stage (at 418-823 K) is much greater than that in the secondary one (at 823-1,123 K) as expressed by a factor of 3.3. The dissociation pressure of most likely present $CaCO_3$ in the residue, and predicted with the aid of line 2 in Fig. 9, amounts to 52.3 kPa at 1,123 K. The authors' experience indicates that this carbonate decomposes quite rapidly under such circumstances.

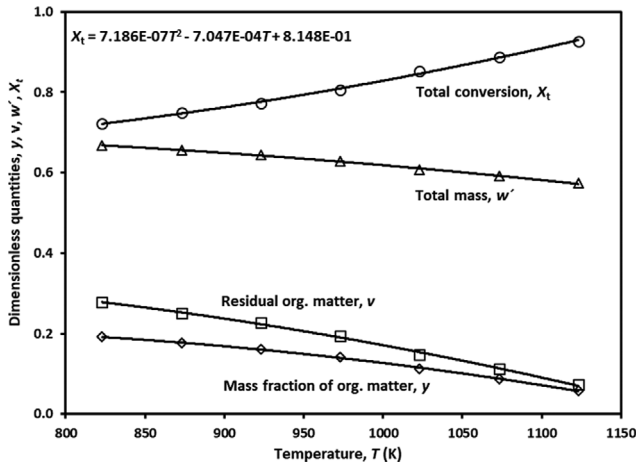

Fig. 10. Plots of normalized TG curves at high temperature.

Analyses of the off-gas showed that the concentrations of its most significant constituents such as CO_2, CO, H_2, and CH_4 at 1,123 K occurred in the ratios 1 : 0.89 : 2.38 : 0.21, respectively. Thermodynamic estimates for the water-gas, the Boudouard and the methanation reaction indicate the prevalence of CO, H_2, and CH_4 above 950, 980, and below 825 K, respectively.

CONCLUSIONS

Municipal sewage sludge is a complex material whose organic part (~50%) includes mainly nonaromatic compounds with the carbon number greater than ~10. A significant fraction of organic matter is constituted by aromates, organic acids, and their esters and salts. The empirical formula of the organic portion is similar to that of a glucose unit laden with nitrogen, sulfur, and chlorine. The intricate thermolysis of the sludge starts in the close vicinity of 418 K. The TG, sigmoidal-shaped, conversion curve levels off at about 823 K with rather slow conversion thereafter. While the principal amount of organic matter (72%) is released at 418-823 K, a minor fraction (21%) is volatilized at a much slower pace at 823-1,123 K.

The off-gas produced at 823 K is composed mainly of CO_2, CO, H_2, and CH_4 in approximate ratios of 1 : 0.23 : 0.62 : 0.26, respectively. Of course, the presence of unwanted compounds such as amines, mercaptans, and chlorophenols is noticeable. The solid residues include about 19% by weight of carbon, are moderately alkaline and do not show any relevant signs of thermoplastic behavior. Their true and apparent density and fractional porosity are as large as 2.20 and 0.836 g cm^{-3}, and 0.62, respectively. The BET surface area amounts to 45.9 $m^2\ g^{-1}$ and is mostly attributed to the mesopores (2-50 nm in diameter). Most abundant components of the sludge ash, produced by oxidizing firing, are (in wt%) SiO_2 (39), CaO (16), Al_2O_3 (13), Fe_2O_3 (13), P_2O_5 (11), MgO (3), and K_2O (2). Dominant minerals are quartz and hematite, with numerous accessories such as feldspars, micas, apatites, and anhydrite.

The course of sludge devolatilization is fairly well modeled by means of the effective kinetics triad inferred from the increasing-temperature experiments: $A=9.396\times10^{-2}\ s^{-1}$, $E/R=3.830\times10^{3}$ K, and n=1.261. The maximum (peak) rate of reaction attained at T_p= 604 K [$u_p \equiv E/(RT_p)$=6.34] amounts to $4.24\times10^{-3}\ K^{-1}$ and the evolved gas consists predominantly of CO_2 with small fractions of CO, H_2, and CH_4. Comparison, e.g., with the well-defined $NaHCO_3$ and $KHCO_3$, shows that the sludge decomposes at much higher temperatures, but still at considerably slower rates. Thus, while the peak temperatures, T_p, of the bicarbonates amount to merely 407 and 422 K, respectively, their top rates of reaction are as large as 2.86×10^{-2} and $3.44\times10^{-2}\ K^{-1}$, respectively. Moreover, the width of the rate curve of sludge at half the peak rate is nearly an order of magnitude greater than those of the bicarbonates. Such wide differences are correspondingly manifested in the greatly different terms $AE/(\beta R)$: 2.16×10^{4} (MSS), 8.45×10^{15} ($NaHCO_3$), and 5.1×10^{20} ($KHCO_3$).

The alternate temperature integral approximation proposed and tested can be employed at the term $u \equiv E/(RT)$ as low as ≥0.1. A

follow-up, explicit relationship presented and validated facilitates predicting the maximum reaction rate temperature, T_p.

As the thermochemical predictions indicate, $MgCO_3$ and $CaCO_3$, most likely to occur in the solids, tend to incipiently dissociate (p_{CO_2}~1 kPa) at approximately 601 and 927 K, respectively. Furthermore, these carbonates are susceptible to being decomposed quite rapidly (p_{CO_2}~50 kPa) at about 749 and 1,164 K, respectively.

The thermolysis offers a promising method to realize the untapped, chemical and fuel potential of municipal sewage sludge. As is to be expected, feasible ways of cleaning the product gas need to be carefully considered.

ACKNOWLEDGEMENTS

This research was supported by the Ministry of Education, Youth, and Sports of the Czech Republic under OP RDE grant No. CZ.02.1.01/0.0/0.0/16_019/0000753 "Research Center for Low-Carbon Energy Technologies" and by the Ministry of Agriculture of the Czech Republic in the 2017-2025 EARTH program under Grant No. QK 21020022 "Complex Evaluation of the Application of Sewage Sludge in Agriculture with Respect to Emerging Pollutants". Mrs. Eva Fišerová is thanked for her aid with the manuscript.

NOMENCLATURE

a : coefficient in integral approximation given by Eq. (6) and in Table 4
A : frequency/pre-exponential factor, fitted parameter [s^{-1}]
A′ : mass fraction of inert inorganic matter in the moisture-free sample of digested sludge
b : coefficient in integral approximation given by Eq. (6) and in Table 4
dX/dT : rate of an nth order reaction in the linearly increasing-temperature mode=$(dX/d\tau)/\beta=k(T)(1-X)^n/\beta$ [K^{-1}]
$(dX/dT)_p$: maximum (peak) rate of reaction corresponding to the inflection point of sigmoidal curve X vs T [K^{-1}]
e : fractional porosity of solid=$(\rho_{He}-\rho_{Hg})/\rho_{He}$
E : apparent (effective) activation energy [J mol^{-1}]
E/R : apparent activation energy term, fitted parameter [K]
I(T) : approximation to the Arrhenius integral=(E/R) p(u) [K]
k : apparent (effective) reaction rate constant=$A\cdot\exp(-u)$ [s^{-1}]
n : apparent order of reaction, fitted parameter
p(u) : dimensionless approximation function
R : ideal gas constant=8.31441 [J mol^{-1} K^{-1}]
T : thermodynamic temperature [K]
T_d : temperature at which the pressure of gaseous reaction product(s) is equal to 101.325 kPa [K]
T_p : peak temperature corresponding to the inflection point of sigmoidal curve X vs T [K]
u : normalized temperature=E/(RT)
v : relative amount of organic matter remaining in the sample= residual amount of organic matter at any moment of time/ initial amount of organic matter=$(w'-A')/(1-A')=1-X_t=A'y/[(1-A')(1-y)]$
V_p : pore volume=$(1/\rho_{Hg})-(1/\rho_{He})=e/\rho_{Hg}$ [cm^3 g^{-1}]
w_o : initial mass of moisture-free sample [g]
$w(\tau)$: mass of the sample at any moment of time [g]
w′ : relative mass of the sample at any moment of time=$w(\tau)/w_0=A'+(1-A')v=A'/(1-y)=1-(1-w'_f)X=1-(1-A')X_t$
w'_f : relative mass of the sample at the end of the process=$w(\tau_f)/w_0$
X : apparent fractional conversion of organic matter from a solid state to a gaseous/vapor state=amount of organic matter released from the sample at any moment of time/amount of organic matter released at the end of the process=$(1-w')/(1-w'_f)=X_t(1-A')/(1-w'_f)$
X_t : true/overall fractional conversion of organic matter from a solid state to a gaseous (vapor) state=amount of organic matter released from the sample at any moment of time/initial total amount of organic matter in the sample=$(1-w')/(1-A')=1-v=(1-y-A')/[(1-A')(1-y)]=X(1-w'_f)/(1-A')$
y : mass fraction of organic matter remaining in the sample at any moment of time=$(w'-A')/w'=v(1-A')/[A'+(1-A')v]=(1-A')(1-X_t)/[1-(1-A')X_t]$
Y(T) : dimensionless integral temperature function=$(A/\beta)\int_0^T[\exp(-u)]dT\cong(A/\beta)I(T)$
Y(X) : dimensionless integral conversion function for an nth order reaction=$\int_0^X dX/(1-X)^n=[1-(1-X)^{1-n}]/(1-n)$

Greek Letters

β : rate of heating [deg s^{-1}]
ρ_{He} : true solid density [g cm^{-3}]
ρ_{Hg} : apparent (particle) density [g cm^{-3}]
τ : elapsed time of reaction/exposure [s]
τ_f : final elapsed time of reaction [s]

REFERENCES

1. D. Zenz, in *Municipal sewage sludge management: A reference text on processing, utilization and disposal*, Lue-Hing, D. R. Zenz, P. Tata, R. Kuchenrither, J. F. Malina Jr. and B. Sawyer, Eds., Vol. 4, 2nd Ed., Technomic, Lancaster (1998).
2. J. Werther and T. Ogada, *Prog. Energ. Combust. Sci.*, **25**, 55 (1999).
3. M. Hartman, K. Svoboda, M. Pohořelý and O. Trnka, *Ind. Eng. Chem. Res.*, **44**, 3432 (2005).
4. M. Hartman, M. Pohořelý and O. Trnka, *Powder Technol.*, **178**, 166 (2007).
5. A. Magdziarz and S. Werle, *Waste Manage.*, **34**, 174 (2014).
6. S. S. A. Syed-Hassan, Y. Wang, S. Hu, S. Su and J. Xiang, *Renew. Sust. Energy Rev.*, **80**, 888 (2017).
7. K. Svoboda, M. Pohořelý, M. Hartman and J. Martinec, *Fuel Process. Technol.*, **90**, 629 (2009).
8. I. Petersen and J. Werther, *Chem. Eng. Process.*, **44**, 717 (2005).
9. G. Liu, M. M. Wright, Q. Zhao and R. C. Brown, *ACS Sustain. Chem. Eng.*, **4**, 1819 (2016).
10. J. Ábrego, J. L. Sanchez, J. Arauzo, I. Fonts, N. Gil-Lalaguna and M. Atienza-Martínez, *Energy Fuel*, **27**, 1026 (2013).
11. I. Fonts, G. Gea, M. Azuara, J. Ábrego and J. Arauzo, *Renew. Sust. Energy Rev.*, **16**, 2781 (2012).
12. S. A. Scott, J. F. Davidson, J. S. Dennis and A. N. Hayhurst, *Chem.*

Eng. Sci., **62**, 584 (2007).
13. M. R. Stammbach, B. Kraaz, R. Hagenbucher and W. Richarz, *Energy Fuel*, **3**, 255 (1989).
14. R. C. Kistler, F. Widmer and P. H. Brunner, *Environ. Sci. Technol.*, **21**, 704 (1987).
15. J. Piskorz, D. S. Scott and I. B. Westerberg, *Ind. Eng. Chem. Process Des. Dev.*, **25**, 265 (1986).
16. T. J. Bandosz and K. Block, *Appl. Catal. B*, **67**, 77 (2006).
17. D. L. Pyle and C. A. Zaror, *Chem. Eng. Sci.*, **39**, 147 (1984).
18. J. Poudel, T. I. Ohm, S. H. Lee and S. C. Oh, *Waste Manage.*, **40**, 112 (2015).
19. M. Atienza-Martínez, J. F. Mastral, J. Ábrego, J. Ceamanos and G. Gea, *Energy Fuel*, **29**, 160 (2015).
20. M. Atienza-Martínez, I. Fonts, J. Ábrego, J. Ceamanos and G. Gea, *Chem. Eng. J.*, **222**, 534 (2013).
21. A. Dhungana, A. Dutta and P. Basu, *Can. J. Chem. Eng.*, **90**, 186 (2012).
22. M. Hartman and O. Trnka, *AIChE J.*, **54**, 1761 (2008).
23. S. A. Scott, J. S. Dennis, J. F. Davidson and A. N. Hayhurst, *Chem. Eng. Sci.*, **61**, 2339 (2006).
24. D. L. Urban and M. J. Antal, *Fuel*, **61**, 799 (1982).
25. J. A. Conesa, A. Marcilla, D. Prats and M. Rodriguez-Pastor, *Waste Manag. Res.*, **15**, 293 (1997).
26. R. Dümpelmann, W. Richarz and M. R. Stammbach, *Can. J. Chem. Eng.*, **69**, 953 (1991).
27. E. Biagini, F. Lippi, L. Petarca and L. Tognotti, *Fuel*, **81**, 1041 (2002).
28. S. A. Scott, J. S. Dennis, J. F. Davidson and A. N. Hayhurst, *Fuel*, **85**, 1248 (2006).
29. A. W. Coats and J. P. Redfern, *Nature*, **201**, 68 (1964).
30. O. Schlömilch, *Compendium der höheren analysis*, 2.-4. Aufl., 2 Bde., Vieweg & Sohn, Braunschweig (1874).
31. C. D. Doyle, *Nature*, **207**, 290 (1965).
32. T. V. Lee and S. R. Beck, *AIChE J.*, **30**, 517 (1984).
33. J. Cai, F. Yao, W. Yi and F. He, *AIChE J.*, **52**, 1554 (2006).
34. G. I. Senum and R. T. Yang, *J. Therm. Anal.*, **11**, 445 (1977).
35. P. Vallet, *Tables numériques permettant l´integration des constantes de vitess par rapport a la température*, Gauthier-Villars, Paris (1961).
36. M. Hartman, K. Svoboda, B. Čech, M. Pohořelý and M. Šyc, *Ind. Eng. Chem. Res.*, **58**, 2868 (2019).
37. M. Hartman, K. Svoboda, M. Pohořelý and M. Šyc, *Ind. Eng. Chem. Res.*, **52**, 10619 (2013).
38. M. R. Othman, Y.-H. Park, T. A. Ngo, S.-S. Kim, J. Kim and K. S. Lee, *Korean J. Chem. Eng.*, **27**, 163 (2010).
39. I. Barin and G. Platzki, *Thermochemical data of pure substances*, 3rd Ed., VCH, Weinheim (1995).
40. M. Hartman and A. Martinovský, *Chem. Eng. Comm.*, **111**, 149 (1992).
41. H. Remy, *Lehrbuch der anorganischen chemie*, Band I, 12th Ed., Geest & Portig, Leipzig (1965).
42. J. Johnston, *J. Am. Chem. Soc.*, **32**, 938 (1910).